Lead distribution in soils impacted by a secondary lead smelter: Experimental and modelling approaches

Arnaud R Schneider, Benjamin Cancès, Marie Ponthieu, Sophie Sobanska, Marc F Benedetti, Olivier Pourret, Alexandra Conreux, Ivan Calandra, Blandine Martinet, Xavier Morvan, et al.

Lead distribution in soils impacted by a secondary lead smelter: experimental and modelling approaches

Arnaud R. SCHNEIDER[a*], Benjamin CANCES[a], Marie PONTHIEU[a], Sophie SOBANSKA[b], Marc F. BENEDETTI[c], Olivier POURRET[d], Alexandra CONREUX[a], Ivan CALANDRA[a], Blandine MARTINET[a], Xavier MORVAN[a], Maxime GOMMEAUX[a], Béatrice MARIN[a]

[a] GEGENAA, EA 3795, Université de Reims Champagne-Ardenne, SFR Condorcet FR CNRS 3417, 2 esplanade Roland Garros, 51100 Reims, France.
[b] Laboratoire de Spectrochimie IR et Raman, UMR-CNRS 8516, Bât. C5 Université de Lille I, 59655 Villeneuve d'Ascq Cedex, France.
[c] Institut de Physique du Globe de Paris, Sorbonne Paris Cité, Université Paris Diderot, UMR 7154, CNRS, F-75005 Paris, France.
[d] HydrISE, Institut Polytechnique LaSalle Beauvais, FR-60000 Beauvais, France.

* Corresponding author
E-mail address: arnaud.schneider@univ-reims.fr (A. Schneider)
Tel.: +33 (0)326773630

Abstract

Smelting activities are one of the most common sources of trace elements in the environment. The aim of this study was to determine the lead distribution in upper horizons (0-5 and 5-10 cm) of acidic soils in the vicinity of a lead-acid battery recycling plant in northern France. The combination of chemical methods (sequential extractions), physical methods (Raman microspectroscopy and scanning electron microscopy with an energy dispersive spectrometer) and multi-surface complexation modelling enabled an assessment of the behaviour of Pb. Regardless of the studied soil, none of the Pb-bearing phases commonly identified in similarly polluted environments (e.g., anglesite) were observed. Lead was mainly associated with organic matter and manganese oxides. The association of Pb with these soil constituents can be interpreted as evidence of Pb redistribution in the studied soils following smelter particle deposition.

Keywords: lead, polluted soils, soil organic matter, manganese oxides.

1 Introduction

The speciation and the lability of trace elements (TE) in soils allow the assessment of their potential mobility and ecotoxicological effects in the environment (Sparks, 2003). Organic matter (OM), clays and metal hydroxides (Al, Fe and Mn) have large and reactive surface areas, making them good scavengers of TE in soils and soil solutions (Hooda, 2010).

Many techniques are available to identify or quantify the relative contributions of the phases involved in Pb retention in soil. For instance, chemical extractions, such as single and sequential extractions (SE), are commonly used to assess the contribution of each adsorptive surface throughout the soil. Many SE procedures exist, and most comprise between 3 and 8 steps to separate different geochemical forms, e.g., exchangeable, acid-soluble, reducible, oxidizable or residual (Tessier et al., 1979; Gleyzes et al., 2002; Rao et al., 2008; Laveuf et al., 2009). Isotopic dilution can be another method to quantify the exchangeable pools of metals in soil (Atkinson et al., 2011; Marzouk et al., 2013). Physical methods, such as scanning electron microscopy coupled with energy dispersive spectrometer (SEM-EDS), Raman microspectroscopy (RMS) and X-ray absorption spectroscopy (XAS), can also be used to fully characterize the TE species in natural systems (Morin et al., 1999; Sobanska et al., 1999; Uzu et al., 2011). Modelling is another approach to determine the TE distribution in the soil. The use of multi-surface complexation models can predict adsorption and ion exchange for various soil constituents (Weng et al., 2001; Cancès et al., 2003; Dijkstra et al., 2004; Pourret et al., 2015; Ren et al., 2015).

Smelting activities are one of the most common sources of TE in the environment (Fernandez-Turiel et al., 2001; Liénard et al., 2014; Ettler, 2016). In the particular case of lead-acid battery recycling, different stages of the process, such as crushing, fusion, reduction and refining, are responsible for emissions of various metals and compounds. Metallic lead (Pb^0), anglesite ($PbSO_4$), lead oxide (PbO) and cerussite ($PbCO_3$) are the predominant species found in the vicinity of lead smelters (Sobanska et al., 1999; Ettler et al., 2005; Ettler et al., 2008; Uzu et al., 2011; Schreck et al., 2012). Particles from primary Pb smelters are composed of relatively insoluble phases (such as $PbSO_4$, $PbSO_4$·PbO, and PbS), while

particulates from secondary Pb smelters are composed of much more soluble phases (such as caracolite, $Na_3Pb_2(SO_4)_3Cl$, and potassium lead chloride, KPb_2Cl_5) (Ettler et al., 2012; Ettler, 2016). Several studies have already addressed the transformation of these Pb-bearing phases in fly ash using batch experiments (Bataillard et al., 2003; Ettler et al., 2005, Ettler et al., 2008, Ettler et al., 2009, Vitkova et al., 2009) or in field conditions using polyamide experimental bags (Ettler et al., 2012). However, very few studies have examined the redistribution of Pb in smelter-impacted soils (e.g., Morin et al., 1999, Ettler et al., 2005).

The objective of the present study was to determine the Pb distribution in the upper horizons of contaminated acidic soils located in the vicinity of a secondary lead smelter. An original approach combining chemical methods (sequential extractions), physical methods (RMS and SEM-EDS) and multi-surface complexation modelling was used to identify Pb phases and to assess the contributions of major reactive components (organic matter, clays, iron and manganese hydroxides) in soils. This approach provides a better understanding and prediction of the behaviour of Pb in smelter-impacted soils.

2 Materials and methods

Soil sampling and characterization

Three heavily contaminated soils were sampled near a secondary lead smelter in northern France (Figure A1; further details on the study area are available in Schneider et al., 2016a). Two of the soils are luvic cambisols (IUSS Working Group WRB, 2014) and developed on Quaternary loam (S1 and S2). The third soil (S3) is a hydromorphic gleysol (IUSS Working Group WRB, 2014) developed on altered upper Cambrian black shales. In this work, only the surficial horizons (A horizon) presenting the highest lead levels were studied. After the litter was removed, two soils samples (0-5 cm: top (T); 5-10 cm: bottom (B)) were collected independently. The six soil samples were stored in polyethylene bags and brought to the laboratory.

The soils were air-dried and sieved through 2 mm mesh. A fraction of the samples was finely crushed for total organic carbon (TOC; NF ISO 14235 (AFNOR, 1998)), total metal content and XRD measurements. The total soil metal contents (Pb, Mn and Fe) were determined by inductively coupled plasma mass spectroscopy (ICP-MS) following tri-acid digestion (HNO_3-$HClO_4$-HF). The soil pH was determined in a mixture of 1:2.5 soil:water (w/v) according to the French standard X 31-103 (AFNOR, 1988). The cation exchange capacity (CEC) was determined by the ammonium acetate saturation method according to the French standard NF-X 31-130 (AFNOR, 1999). Finally, the clay, silt and sand contents were determined by the pipette method following the French standard NF-X 31-107 (AFNOR, 2003).

Sequential Extraction

To estimate the chemical partitioning of Pb in the six soil samples, an SE procedure comprising eight steps, adapted from Laveuf et al. (2009), was used (Table 1). The extractions were made in triplicate on 1 g of sieved (2 mm), air-dried soil in polypropylene tubes. After each extraction step, the tubes were centrifuged at 3000 g for 20 min. The supernatants were filtered (0.2 µm) and stored at 4°C prior to analysis. The residues were washed with 10 mL of ultrapure water (Milli-Q, 18.2 mΩ). A blank experiment was run at the same time as each

extraction procedure. Because of the very high TOC contents in the soil samples, the 4th step of the SE was repeated three times. All the supernatants were acidified with ultrapure HNO_3 before analysis via inductively coupled plasma atomic emission spectroscopy (ICP-AES).

X-ray diffraction

Bulk soil samples of the three topsoils (S1T, S2T and S3T) were wet-sieved at 500, 200, 50 and 20 μm in deionized water, without preliminary treatments. The remaining fractions (< 20 μm) were further fractionated by sedimentation in deionized water according to Stokes law. The particle-size fractions obtained were < 2, 2-20, 20-50, 50-200, 200-500 and 500-2000 μm.

The mineralogical compositions of the fine fraction (< 2 μm) of the three topsoil samples were determined by X-ray powder diffraction analysis. A Bruker AXS D8 diffractometer using Cu-Kα radiation and operating in step scan mode between 3 and 70° 2θ with 0.04° 2θ steps and a counting time of 10 s per step was used. The identification and quantification of mineral phases was performed using Diffrac Eva software and the ICDD Database (2003).

Scanning electron microscope with an energy dispersive spectrometer

The morphology and elemental distribution of the Pb-enriched areas of the three topsoil samples (S1T, S2T and S3T) were investigated with a Hitachi TM-1000 and a Hitachi S3400 scanning electron microscope (SEM) equipped with an energy dispersive spectrometer (EDS). The bulk soil samples and size fractions with high Pb contents (determined with a field portable X-ray fluorescence instrument, data not shown) were directly mounted on a stub or embedded in GEOFIX epoxy resin and prepared as thin sections for microscopic observations.

Raman microspectroscopy

The RMS technique was used to provide molecular characterization of Pb-host phases in the three topsoil samples. RMS measurements were carried out using a LabRAM HR Evolution confocal Raman microspectrometer (Horiba, Jobin Yvon) equipped with a 785 nm wavelength laser beam, with an energy of 8 mW at the sample surface, a back illuminated liquid-nitrogen-cooled charge-coupled device (CCD) detector (1024×512 pixels) and a microscope objective (Olympus BX40; 100×, 0.8 NA) in the backscattering mode. A video camera provided an optical view of the samples. The spot size of the laser focused by the objective at the surface of sample was estimated to be of the order of 1 μm^2 in the XY plane. Measurements were focused on metal-enriched areas previously observed by SEM-EDS after a careful relocation. For identification of molecular species, the experimental spectra (Raman band positions and relative intensities) were compared with reference spectra of pure (anglesite, cerussite and Pb oxides) and synthetic compounds. Goethite (α-FeOOH) and ferrihydrite were synthetized according to Schwertmann and Cornell (2000) and hydrous manganese oxides (HMO) were synthetized according to Gadde and Laitinen (1974). Adsorption of Pb(II) on synthetic goethite, ferrihydrite and HMO was achieved following the method described by Xu et al. (2006). This procedure yielded HMO and ferrihydrite samples with 5 wt % of Pb and goethite samples with 2 wt % of Pb. The total amount of metal

adsorbed was calculated from a mass balance by subtracting the final aqueous concentration from the initial one after filtration at 0.2 µm.

Donnan Membrane Technique and dissolved organic carbon fractionation

The total and free concentrations of Pb, as well as the dissolved organic carbon (DOC) in the soil solution, were measured in the six soil samples following a soil-column Donnan membrane technique (SC-DMT; Temminghoff et al., 2000) with 2.10^{-3} mol.L^{-1} $Ca(NO_3)_2$ as background electrolyte at a soil:solution ratio of 80 g.L^{-1} (Schneider et al., 2016b). According to the batch technique of Van Zomeren and Comans (2007), dissolved organic matter (DOM) was fractionated into humic acids (HA), fulvic acids (FA), hydrophilic acids (Hy), and hydrophobic neutral organic matter (HON) (more details are given in Schneider et al., 2016b). In this study, the reactive DOM was assumed to be the measured FA fraction. This fraction represents between 21.1% and 27.3% of the total DOM (Schneider et al., 2016b).

Multi-surface complexation modelling

In this study, a multi-surface complexation model was used to describe the metal partitioning in the six soil samples. Different sub-models were used to describe metal adsorption on organic and inorganic surfaces. All the calculations were made with ECOSAT (Keizer and Van Riemsdijk, 1999).

An ion exchange model was used to calculate TE adsorption on clays according to the Gaines-Thomas convention (Appelo and Postma, 1996).

The binding of metal to amorphous iron oxides (amor-Fe) was estimated with the two-site surface complexation diffuse-double layer (DDL) model using generic parameters from Dzombak and Morel (1990). The amounts of amor-Fe were estimated with the Fe proportions extracted with the 5th fraction of the SE (F5: bound to amorphous iron oxides; Table 1). The amor-Fe was assumed to be ferrihydrite, with a molecular weight of 481 g.mol^{-1} and a specific surface area of 600 m^2.g^{-1} (Dzombak and Morel, 1990). The amount of crystalline iron oxides (cry-Fe) was estimated with the 6th fraction of the SE (F6: bound to crystalline iron oxides; Table 1) and was assumed to be goethite, with a molecular weight of 88.9 g.mol^{-1} and a specific surface area of 50 m^2.g^{-1} (Weng et al., 2001). The modelled proportions of Pb associated with goethite using the CD-MUSIC model and the generic parameters from the literature (Hiemstra and Van Riemsdijk, 1996; Ponthieu et al. 2006) were negligible as they represented less than 0.1% of the total Pb content of the soil. For this reason, the cry-Fe was not taken into account in the following results and discussion.

Metal binding to hydrous manganese oxides (HMO) was described by the 2-pK diffuse layer model with a molecular weight of 119 g.mol^{-1} and a specific area of 746 m^2.g^{-1} using generic parameters from Tonkin et al. (2004). The amount of HMO was estimated with the proportion of Mn extracted in the 3rd step of the SE (F3: bound to manganese oxides; Table 1).

Finally, metal binding to the dissolved organic matter (DOM) and soil organic matter (SOM) was described with the non-ideal competitive adsorption Donnan model (NICA-Donnan; Kinniburgh et al., 1999). The reactive DOM was assumed to be fulvic acids (Schneider et al., 2016b), and the reactive SOM was assumed to be humic acids (Weng et al., 2001; Ren et al., 2015). The reactive content of DOM, i.e., the fulvic acids fraction, was measured according to the batch technique of Van Zomeren and Comans (2007).

The reactive content of SOM was calculated following Weng et al. (2001). SOM and clays are the main constituents that contribute to the soil CEC. The clay content (< 2 µm) was used as an estimate of the clay minerals content in the soil. To calculate the contribution of clay minerals to the soil CEC, average CEC values (an average CEC for each clay mineral identified by XRD) were used: 0.25, 0.09, 0.3 and 0.25 $mol.kg^{-1}$ for muscovite, kaolinite, chlorite and illite, respectively (Sparks, 2003). The CEC due to SOM was then obtained by subtracting the clay-related CEC from the measured soil CEC. Finally, the site densities of HA, as defined by Milne et al. (2003), were used to estimate the proportion of reactive SOM as HA.

Based on a large collection of data, Milne et al. (2003) derived "generic" parameters for the NICA-Donnan model to describe proton and metal ions binding to FA and HA. These generic parameters have succeeded in producing reasonable predictions over a wide range of environmental conditions for metal ions such as Cd and Cu but are more controversial for Pb (Weng et al., 2001; Cancès et al., 2003; Bonten et al., 2008). Xiong et al. (2013) defined new generic parameters to describe proton and Pb binding to FA and HA. In this study, we compared the Pb distribution modelling using the parameters from Milne et al. (2003) with that obtained using the parameters from Xiong et al. (2013) (Table A1).

Model inputs were (i) soil solution pH; measured FA; free Cd, Cu, Pb and Zn activities; and Ca, NO_3, Na and Cl concentrations in the soil solutions (as measured with SC-DMT; Table A2), and (ii) the concentrations of reactive sorption surfaces in the soil samples.

3 Results

The soil physicochemical properties are presented in Table 2. Their mineral compositions and their reactive sorption surfaces are listed in Table 3. The six soil samples are acidic, with pH values between 4.3 and 4.6. The S1 and S2 soil samples exhibit moderate SOM contents (between 9.4 and 20.6%), while the S3 soil samples show very high SOM contents (49.8% in S3T and 47.9% in S3B). The soil CEC ranges from 14.7 to 61.9 $cmol.kg^{-1}$ and is significantly correlated with the SOM contents ($R^2 = 0.998$, $p < 0.001$). The six soil samples are heavily contaminated with Pb, with contents ranging from 881 to 9034 $mg.kg^{-1}$. The Pb content is higher in the S1 and S2 topsoil samples than in the deeper samples, whereas the content increases slightly with depth in S3.

Geochemical partitioning of Pb

The exchangeable (F1) and acid-soluble (F2) fractions of Pb represent between 32.5% and 49.7% of the total Pb content in the soil samples (Figure 1). The proportion of Pb extracted with the exchangeable fraction (F1) is higher for S1 and S2 (between 1.3% and 2% of the total Pb) than for S3 (0.5% of the total Pb). The acid-soluble fraction is the most important in S1 and S2 (between 37% and 48%), whereas Pb is mainly released in the easily oxidisable fraction (F4) in S3 (48% for S3 and 14-27% for S1 and S2; Table A3). These results suggest that Pb is mainly associated with organic matter in S3 and are consistent with the high SOM values in these two soil samples (Table 2).

The fraction of Pb bound to manganese oxides (F3) in S1 and S2 ranges from 14% to 20%, while it only ranges from 2.4% to 3.5% in S3. However, the highest proportions of

manganese oxides occur in S2 (S2T: 51% and S2B: 27%) and S3 (S3T: 43%), which have the highest total Mn contents (Table 2 and Table A3).

For all soil samples, the proportion of Pb bound to amorphous iron oxides (F5; between 5.7% and 11%) is always higher than that bound to crystalline iron oxides (F6; between 1.3% and 3.8%). The total Fe contents are slightly higher for the S3 soil samples (Table 2), but the proportions of iron corresponding to amorphous and crystalline iron oxides are similar in the 6 soil samples (Table A3).

Finally, the oxidisable fraction (F7) is negligible (< 0.3% of total Pb), and the residual fraction (F8) ranges from 3% to 14% of the total Pb.

Chemical associations of Pb at the micrometre scale

In the six soil samples, no Pb-bearing minerals could be identified by XRD. Although $PbSO_4$, $PbCO_3$, KPb_2Cl_5 and $Na_3Pb_2(SO_4)_3Cl$ are known to be the major particulate phases directly rejected by a secondary lead smelter (Ettler, 2016), these Pb-rich phases were not observed.

The selected soil samples were imaged and analysed by SEM-EDS to better constrain the Pb distribution within the host phases and the chemical associations between Pb and other elements at the microscopic scale. Although soils are very complex and heterogeneous at this scale, the main observed elemental association is Pb-Mn. In all the studied soil samples, Pb-rich areas systematically correspond to Mn-rich areas. Elemental maps of a topsoil thin section indicate that Pb is mainly concentrated in Mn-rich heterogeneous aggregates (Figure 2). In this sample, Pb also seems to be partially associated with Fe. However, in the three studied soils, this association was rarely observed, and the main association was Pb-Mn. These Pb-Mn-rich phases are present in soil aggregates (Figure 3b) or at the surface of plant debris (Figures 3a and 3c). Manganese-rich precipitates on needle litter colonized by fungi have already been observed in previous studies (Blanchette, 1984; Keiluweit et al., 2015).

To determine the exact nature of these phases identified by SEM-EDS, Pb-rich areas of the three topsoils (0-5 cm) were analysed by RMS and compared with reference samples (Figure 3). The Raman spectra of all the observed areas are very similar, which indicates that the rich-Pb phases are the same regardless of the studied soil sample. The Raman spectra are mainly characterized by a large Raman band at 640 cm^{-1}, and they agree well with the typical Raman spectra of synthesized amorphous manganese oxide with adsorbed Pb (Figure 3). Notably, no other Pb compounds, such as $PbSO_4$, $PbCO_3$ or PbO, which are typical compounds found in soils in the vicinity of secondary Pb smelters, were identified by RMS.

All these observations at the micrometre scale clearly suggest that the Pb association with manganese oxides occurs in the soils of the studied site. However, diffuse forms of Pb in the soil matrix, for instance, in association with organic matter as suggested by the sequential extraction results, are difficult to identify by RMS and SEM-EDS. To overcome this limitation, a modelling approach was undertaken.

Modelling of Pb distribution

The free Pb activity in the soil solutions was used as model input data to estimate the content of Pb in the soil solution and in the soil, as well as its partitioning among the different reactive phases in the 6 soil samples. The calculated total Pb concentrations in the soil solution are very close to the total Pb concentrations measured in the soil solution, regardless of the

parameters used to describe Pb-FA interactions in the generic NICA-Donnan model (from Milne et al., 2003 or Xiong et al., 2013). The speciation of Pb in the soil solution is not detailed here, as it is fully discussed in Schneider et al. (2016b).

For the six soil samples, the calculated proportions of reactive SOM as HA (between 18.5 and 22.1% of the total SOM content) are consistent with previous results obtained by Weng et al. (2001; 16-46%) and Ren et al. (2015; 7-55%).

The modelling results obtained with the generic NICA-Donnan parameters from Milne et al. (2003) and from Xiong et al. (2013) were compared (Table A1, Table 4). The model calculations indicated that soil organic matter is the main sorbent of Pb in soils. The Pb associated with SOM represents between 72% and 97% and between 87% and 99% of the total Pb, according to the parameters of Milne et al. (2003) and Xiong et al. (2013), respectively (Table 4). The only difference when using the two set of parameters for the NICA-Donnan model concerns the Pb content associated with SOM (HA) and therefore the total Pb content in the soil. Indeed, the amount of Pb associated with clays, HFO and HMO did not change (Table 4). Using the parameters of Xiong et al. (2013), the quantity of Pb associated with HA is more important than when the parameters of Milne et al. (2003) are used, with a consequential increase in the total Pb content associated with the soil solid phases (between 2.1 and 2.7 times more). Consequently, the proportion of Pb-HMO interactions is larger using the parameters of Milne et al. (2003) than the parameters of Xiong et al. (2013) and represents up to 25% and 12% of total Pb, respectively. The proportion of the nonspecific adsorption on clay surfaces is small and represents between 1.1% and 5.3% with the parameters of Milne et al. (2003) and between 0.5% and 2.2% with the parameters of Xiong et al. (2013). Finally, less than 1% of adsorbed Pb is attributed to HFO.

4 Discussion

Influence of model parameters on total Pb content prediction

The total Pb contents modelled with the free Pb activities as input data were lower than the measured total Pb contents in the soil. It is well known that the total metal content is not active in adsorption processes (Weng et al. 2001; Ren et al. 2015), yet the multi-surface complexation models are only able to describe the geochemically reactive metal contents. In most modelling studies, 0.43 M HNO_3 is used to estimate the TE contents that the model calculation is able to distribute between the different solid phases in the soil (Weng et al., 2001; Dijkstra et al., 2004; Ren et al., 2015). Other extractants, such as EDTA buffered at a pH of 4.65, have also been used (Bonten et al., 2008; Pourret et al., 2015). In this study, the geochemically reactive Pb content is assumed to be the sum of the Pb extracted in the first six SE fractions (F1 to F6). The multi-surface complexation model should be able to describe the processes involved in the retention of Pb extract with these six fractions.

Because soil organic matter is the major sorbent of Pb in the studied soils, the choice of the NICA-Donnan generic parameters has an important impact on the total modelled Pb content. When the NICA-Donnan parameters are taken from Milne et al. (2003), the total modelled Pb contents are substantially lower than those modelled with the parameters from Xiong et al. (2013) (Table 4). Xiong et al. (2013) defined higher affinity constants for Pb in the two reactive sites of HA than Milne et al. (2003), which explains the discrepancy (Table A1).

Regardless of the modelled lead distribution, the Xiong et al. (2013) parameters seem more appropriate than the Milne et al. (2003) parameters for estimating the total Pb content distributed amongst the different solid phases of the soil measured with the first six SE fractions. The use of the Xiong et al. (2013) parameters allows a satisfactory description of the geochemically reactive Pb content (between 55% and 122% of the measured Pb in the F1 to F6 fractions), considering that the modelling input data are the free Pb activities measured in the soil solution.

The model predicted a major association between Pb and organic matter, while the SE and the spectroscopic data indicated the importance of HMO and, to a lesser extent, HFO in the Pb partitioning in the soils. A possible explanation of this difference could be that the reactivities of HMO and/or HFO were underestimated by the modelling.

Role of clays

The interactions of Pb with clay minerals have been evidenced by the modelling, even if they represent less than 6% of the geochemically reactive Pb. The adsorption of Pb on the clay minerals is described with an ion exchange model, which only considers weak associations. This Pb fraction should therefore be comprised in the exchangeable fraction (F1) of the SE. To compare the predicted weakly bound Pb with the F1 results, several modelled fractions of Pb have to be considered: total Pb in the soil solution, Pb adsorbed on clays, and Pb electrostatically bound to HA and oxides. The sum of all these modelled fractions is higher than the measured Pb exchangeable fraction. However, when only the sum of the modelled total soil solution Pb and Pb adsorbed on clays is considered, a good agreement is observed with the measured Pb exchangeable fraction (with a slope of 0.90 and a R^2 of 0.91), although Pb electrostatically bound to HA and to oxides was not considered. An explanation could be (i) an overestimation of the Pb-clay fraction estimated with the ion exchange model or (ii) an extraction of Pb electrostatically bound to HA and oxides during the acid-soluble step of the SE (F2; Gleyzes et al., 2002).

Role of soil organic matter and manganese oxides

The major particulate phases emitted by secondary lead smelters are known to be caracolite ($Na_3Pb_2(SO_4)_3Cl$), lead chloride ($PbCl_2$) and potassium lead chloride (KPb_2Cl_5) (Ettler, 2016). Several studies have shown that most of these phases are highly soluble, especially in acidic conditions, and anglesite ($PbSO_4$) and lead sulfite ($PbSO_3$) are formed as their main final and stable alteration products (Ettler et al., 2005; Ettler et al., 2008; Vitkova et al., 2009). However, few studies have dealt with the identification and transformation of these phases in soils and little is known about the fate of Pb that is not trapped by the precipitation of secondary phases. In this work, Pb-bearing crystalline phases were not observed. Although this result does not rule out the possible occurrence of small amounts of crystalline Pb phases (e.g., anglesite), it suggests that Pb is mainly present as non-crystalline Pb-bearing species and/or that the proportion of crystalline phases is below the detection limit of XRD.

In all the studied soils, despite different soil types and levels of contamination, Pb is mainly associated with organic matter and manganese oxides. The very large proportion of Pb associated with SOM is consistent with previous studies in which SOM was the most important sorption surface for Pb in soils (Lofts and Tipping, 1998; Morin et al., 1999; Weng

et al., 2001; Bataillard et al., 2003). The large modelled proportions of Pb bound to SOM are not coherent with the SE results in which Pb is more distributed between several fractions and a large part is extracted during the acid-soluble step. This discrepancy could be explained by a lack of selectivity during the acid-soluble step with a non-negligible portion of the Pb specifically bound to the surface of clays, Fe/Mn oxides and organic matter likely extracted during this second step of the SE (Gleyzes et al., 2002; Young et al., 2006).

The modelling and the SE results indicated a non-negligible fraction of Pb associated with manganese oxides. These results are consistent with SEM-EDS and RMS observations, which highlighted the presence of Pb-manganese oxides associations. The modelled and measured proportions of Pb associated with manganese oxides are similar in the S2 soil samples, which present the highest proportions of manganese oxides (Table 3). Significant proportions of manganese oxides are also observed in the S3 soil samples, and the lower (measured and modelled) fraction of Pb bound to manganese oxides is explained by the very high organic matter content. The manganese oxide contents in the S1 soil samples are lower than those in S2 and S3, explaining the lower proportions calculated by the model. However, the measured proportions of Pb bound to HMO (F3 of SE, Table A3) in S1 are similar to that measured in S2. This result could be explained by a lack of selectivity of the SE or, more hypothetically, by a different reactivity of the manganese oxides of the S1 soil samples (Nelson et al., 1999). Nonetheless, our results suggest that manganese oxides contribute significantly to Pb distribution in acidic impacted soils. The importance of manganese oxides in Pb distribution in soils has already been studied (e.g., Fan et al., 2005; Xu et al., 2006) and directly evidenced by X-ray absorption spectroscopy in the surface horizons of wooded soils (Morin et al., 1999). Some studies also reported the role of iron oxides in Pb retention in soil (Ettler et al., 2005). In this study, these mineral phases are not significantly involved in Pb distribution (i.e., less than 1%). Even if manganese oxides are present at much lower concentrations than amorphous iron oxides in the studied soil samples (Table 3), their reactivity is higher (Table 4). The adsorption of Pb on manganese oxide minerals starts at very low pH values ($pH < 3$; Gadde and Laitinen, 1974; Smith, 1999; Fan et al., 2005). At pH values similar to those in the studied soil (pH values of 4 to 5), the adsorption of Pb on other oxides (Fe and Al) is always lower because of their higher pH_{zpc}. Michalkova et al. (2014) and Ettler et al. (2015) recently demonstrated that amorphous manganese oxides (AMO) can be used as an amendment in Pb smelter-polluted agricultural soils to decrease the labile fraction of Pb. They showed that these mineral phases were very efficient at acidic pH values of 4-5. Moreover, several studies have also found that biotic manganese oxides are more reactive than abiotic manganese oxides (Nelson et al., 1999; Saratovsky et al., 2006; Miyata et al., 2007). Nelson et al. (1999) noted that Pb adsorption on biogenic manganese oxide was two to five times greater than the Pb adsorption on a chemically precipitated abiotic manganese oxide. The characterization of biotic manganese oxides is however difficult without additional techniques, such as transmission electron microscopy (TEM) and extended X-ray absorption fine structure (Kim et al., 2003).

5 Conclusion

By combining experimental and modelling approaches, this study emphasizes the role of SOM, and, to a lesser degree, of manganese oxides in the scavenging of Pb in heavily impacted soils. Although crystalline Pb phases are frequently cited as important Pb-bearing phases emitted by lead smelters, none were observed in the acidic soils of this study. The association of Pb with organic matter and manganese oxides can be interpreted as evidence of Pb redistribution in the studied soils after smelter particles deposition. The affinity of Pb with these phases is already known, but direct evidence of the Pb association with manganese oxides in soils has rarely been highlighted. Further studies are needed to clarify the exact nature (abiotic or biotic) of the manganese oxides in order to better model their reactivities and interactions with Pb in the soil.

Acknowledgements

This study was supported by the Champagne-Ardenne region (France). The authors acknowledge Stéphanie Rossano and Chloé Fourdrin (Laboratoire Géomatériaux et Environnement, Université Paris-Est Marne-la-Vallée), Céline Rousse and Patrick Fricoteaux (Laboratoire d'Ingénierie et Sciences des Matériaux, Université de Reims Champagne-Ardenne) for the XRD analyses. We also thank Thomas Salmon and Sandrine Jégou (Laboratoire d'œnologie et Chimie Appliquée, Université de Reims Champagne-Ardenne) for freeze-drying the synthetic samples.

References

AFNOR (1988) Détermination du pH dans l'eau. NFX 31-103.

AFNOR (1998) Qualité du sol, Dosage du carbone organique par oxydation sulfochromique. NF ISO 14235.

AFNOR (1999) Détermination de la Capacité d'Echange Cationique (CEC) et des cations extractibles. NF X 31-130.

AFNOR (2003) Qualité des sols, analyse granulométrique par sédimentation, Méthode de la pipette. NF X 31-107 standard.

Appelo CAJ, Postma D (1996) Geochemistry, Groundwater and Pollution. Balkema Publishers, Rotterdam.

Atkinson NR, Bailey EH, Tye AM, Breward N, Young D (2011) Fractionation of lead in soil by isotopic dilution and sequential extraction. Environmental Chemistry 8(5): 493-500.

Bataillard P, Cambier P, Picot C (2003) Short-term transformations of lead and cadmium compounds in soil after contamination. European Journal of Soil Science 54: 365-376.

Blanchette RA (1984) Manganese accumulation in wood decayed by white rot fungi. Phytopathology 74(6): 725-730.

Bonten LTC, Groenenberg JE, Weng L, Van Riemsdijk WH (2008) Use of speciation and complexation models to estimate heavy metal sorption in soils. Geoderma 146: 303-310.

Cancès B, Ponthieu M, Castrec-Rouelle M, Aubry E, Benedetti MF (2003) Metal ions speciation in a soil and its solution: experimental data and model results. Geoderma 113: 341-355.

Dijkstra JJ, Meeussen JCL, Comans RNJ (2004) Leaching of heavy metals from contaminated soils: an experimental and modeling study. Environmental Science and Technology 38: 4390-4395.

Dzombak DA, Morel FMM (1990) Surface Complexation Modeling: Hydrous Ferric Oxides. John Wiley & Sons, 393p.

Ettler V, Vanek A, Mihaljevic M, Bezdicka P (2005) Contrasting lead speciation in forest and tilled soils heavily polluted by lead metallurgy. Chemosphere 58: 1449-1459.

Ettler V, Sebek O, Grygar T, Klementova M, Bezdička P, Slavíková H (2008) Controls on metal leaching from secondary Pb smelter air-pollution-control residues. Environmental Science and Technology 42: 7878-7884.

Ettler V, Vrtiskova R, Mihaljevic M, Sebek O, Grygar T, Drahota P (2009) Cadmium, lead and zinc leaching from smelter fly ash in simple organic acids-Simulators of rhizospheric soil solutions. Journal of Hazardous Materials 170: 1264-1268.

Ettler V, Mihaljevic M, Sebek O, Grygar T, Klementova M (2012) Experimental in Situ Transformation of Pb Smelter Fly Ash in Acidic Soils. Environmental Science and Technology 46 (19): 10539-10548.

Ettler V, Tomasova Z, Komarek M, Mihaljevic M, Sebek O, Michalkova Z (2015) The pH-dependent long-term stability of an amorphous manganese oxide in smelter-polluted soils: Implication for chemical stabilization of metals and metalloids. Journal of Hazardous Materials 286: 386-394.

Ettler V (2016) Soil contamination near non-ferrous metal smelters: A review. Applied Geochemistry 64: 56-74.

Fan M, Boonfueng T, Xu Y, Axe L, Tyson TA (2005) Modeling Pb sorption to microporous amorphous oxides as discrete particles and coatings. Journal of Colloid and Interface Science 281: 39-48.

Fernandez-Turiel JL, Aceñolaza P, Medina ME, Llorens JF, Sardi F (2001) Assessment of a smelter impact area using surface soils and plants. Environmental Geochemistry and Health 23: 65-78.

Gadde RR, Laitinen HA (1974). Heavy metal adsorption by hydrous iron and manganese oxides. Analytical Chemistry 46 (13): 2022-2026.

Gleyzes C, Tellier S, Astruc M (2002) Fractionation studies of trace elements in contaminated soils and sediments: a review of sequential extraction procedures. TrAC Trends in Analytical Chemistry 21: 451-467.

Hiemstra T, Van Riemsdijk WH (1996) A Surface Structural Approach to Ion Adsorption: The Charge Distribution (CD) Model. Journal of Colloid and Interface Science 179: 488-508.

Hooda PS (2010) Trace Elements in Soils, Wiley, London, p. 618.

ICDD (2003) JCPDS PDF-2 database, Newton Square, PA, U.S.A.

IUSS Working Group WRB (2014). World reference base for soil resources, International Soil Classification System for Naming Soils and Creating Legends for Soil Maps, FAO, Rome, http://www.fao.org/3/a-i3794e.pdf.

Keiluweit M, Nico P, Harmon ME, Mao J, Pett-Ridge J, Kleber M (2015) Long-term litter decomposition controlled by manganese redox cycling. Proceedings of the National Academy of Sciences 112(38): E5253-E5260.

Keizer MG, Van Riemsdijk WH (1999) ECOSAT: Equilibrium Calculation of Speciation and Transport, User Manual, Version 4.7. Wageningen Agricultural University, The Netherlands.

Kim HS, Pasten PA, Gaillard JF, Stair PC (2003) Nanocrystalline Todorokite-Like Manganese Oxide Produced by Bacterial Catalysis. Journal of American Chemical Society 125: 14284-14285.

Kinniburgh DG, van Riemsdijk WH, Koopal LK, Borkovec M, Benedetti MF, Avena MJ (1999) Ion binding to natural organic matter: competition, heterogeneity, stoichiometry and thermodynamic consistency. Colloids and Surfaces A: Physicochemical and Engineering Aspects 151 (1-2): 147-166.

Laveuf C, Cornu S, Baize D, Hardy M, Josiere O, Drouin S, Bruand A, Juillot F (2009) Zinc Redistribution in a Soil Developed from Limestone During Pedogenesis. Pedosphere 19(3): 292-304.

Liénard A, Brostaux Y, Colinet G (2014) Soil contamination near a former Zn-Pb ore-treatment plant: Evaluation of deterministic factors and spatial structures at the landscape scale. Journal of Geochemical Exploration 147: 107-116.

Lofts S, Tipping E (1998) An assemblage model for cation binding by natural particulate matter. Geochimica et Cosmochimica Acta 62: 2609-2625.

Marzouk ER, Chenery SR, Young SD (2013) Measuring reactive metal in soil: a comparison of multi-element isotopic dilution and chemical extraction. European Journal of Soil Science 64: 526-536.

Michalkova Z, Komarek M, Sillerova H, Della Puppa L, Joussein E, Bordas F, Vanek A, Vanek O, Ettler V (2014) Evaluating the potential of three Fe- and Mn-(nano)oxides for the stabilization of Cd, Cu and Pb in contaminated soils. Journal of Environmental Management 146: 226-234.

Milne CJ, Kinniburgh DG, van Riemsdijk WH, Tipping E (2003) Generic NICA-Donnan model parameters for metal ion binding by humic substances. Environmental Science and Technology 37: 958-971.

Miyata N, Tani Y, Sakata M, Iwahori K (2007) Microbial Manganese Oxide Formation and Interaction with Toxic Metal Ions. Journal of Bioscience and Bioengineering 104: 1-8.

Morin G, Ostergren JD, Juillot F, Ildefonse P, Calas G, Brown Jr GE (1999) XAFS determination of the chemical form of lead in smelter-contaminated soils and mine tailings: Importance of adsorption processes. American Mineralogist 84: 420-434.

Nelson YM, Lion LW, Ghiorse WC, Shuler ML (1999) Production of Biogenic Mn Oxides by Leptothrix discophora SS-1 in a Chemically Defined Growth Medium and Evaluation of Their Pb Adsorption Characteristics. Applied and Environmental Microbiology 65: 175-180.

Ponthieu M, Juillot F, Hiemstra T, Van Riemsdijk WH, Benedetti MF (2006) Metal ion binding to iron oxides. Geochimica et Cosmochimica Acta 70: 2679-2698.

552 Pourret O, Lange B, Houben D, Colinet G, Shutcha M, Faucon MP (2015) Modeling of cobalt
553 and copper speciation in metalliferous soils from Katanga (Democratic Republic of
554 Congo). Journal of Geochemical Exploration 149: 87-96.
555 Rao CRM, Sahuquillo A, Lopez Sanchez JF (2008) A review of the different methods applied
556 in environmental geochemistry for single and sequential extraction of trace elements in
557 soils and related materials. Water, Air, and Soil pollution 189 (1): 291-333.
558 Ren ZL, Sivry Y, Dai J, Tharaud M, Cordier L, Benedetti MF (2015) Multi-element stable
559 isotopic dilution and multi-surface modelling to assess the speciation and reactivity of
560 cadmium and copper in soil. European Journal of Soil Science 66 (6): 973-982.
561 Saratovsky I, Wightman PG, Pasten PA, Gaillard JF, Poeppelmeier KR (2006) Manganese
562 Oxides: Parallels between Abiotic and Biotic Structures. Journal of American Chemical
563 Society 128: 11188-11198.
564 Schneider AR, Morvan X, Saby NPA, Cancès B, Ponthieu M, Gommeaux M, Marin B
565 (2016a) Multivariate spatial analyses of the distribution and origin of trace and major
566 elements in soils surrounding a secondary lead smelter. Environmental Science and
567 Pollution Research: In press.
568 Schneider AR, Ponthieu M, Cancès B, Conreux A, Morvan X, Gommeaux M, Marin B,
569 Benedetti MF (2016b) Influence of dissolved organic matter and manganese oxides on
570 metal speciation in soil solution: a modelling approach. Environmental Pollution 213:
571 618-627.
572 Schreck E, Foucault Y, Sarret G, Sobanska S, Cecillon L, Castrec-Rouelle M, et al. (2012)
573 Metal and metalloid foliar uptake by various plant species exposed to atmospheric
574 industrial fallout: Mechanisms involved for lead. Science of the Total Environment 427-
575 428: 253-262.
576 Schwertmann U, Cornell RM (2000) Iron oxides in the laboratory: preparation and
577 characterization, 2nd ed. Wiley-VCH, Weinheim.
578 Smith KS (1999) Metal sorption on mineral surfaces an overview with examples relating to
579 mineral deposits. U.S. Geological Survey, Box 25046, MS 973, Federal Center, Denver.
580 Sobanska S, Ricq N, Laboudigue A, Guillermo R, Bremard C, Laureyns J, et al. (1999)
581 Microchemical investigations of dust emitted by a lead smelter. Environmental Science
582 and Technology 33:1334-1339.
583 Sparks DL (2003) Environmental Soil Chemistry, 2nd ed. Academic Press, San Diego, CA.
584 Temminghoff EJM, Plette ACC, Van Eck R, Van Riemsdijk WH (2000) Determination of the
585 chemical speciation of trace metals in aqueous systems by the Wageningen Donnan
586 Membrane Technique. Analytica Chimica Acta 417 (2): 149-157.
587 Tessier A, Campbell PGC, Bisson M (1979) Sequential extraction procedure for the
588 speciation of particulate trace metals. Analytical Chemistry 51 (7): 844-851.
589 Tonkin JW, Balistrieri LS, Murray JW (2004) Modeling sorption of divalent metal cations on
590 hydrous manganese oxide using the diffuse double layer model. Applied Geochemistry
591 19: 29-53.
592 Uzu G, Sobanska S, Sarret G, Sauvain JJ, Pradere P, Dumat C (2011) Characterization of
593 lead-recycling facility emissions at various workplaces: Major insights for sanitary risks
594 assessment. Journal of Hazardous Materials 186:1018-1027.

595 Van Zomeren A. Comans RNJ (2007) Measurement of humic and fulvic acid concentrations
596 and dissolution properties by a rapid batch procedure. Environmental Science and
597 Technology 41: 6755-6761.
598 Vítkova M; Ettler V; Sebek O; Mihaljevic M; Grygar T; Rohovec J (2009) The pH-dependent
599 leaching of inorganic contaminants from secondary lead smelter fly ash. Journal of
600 Hazardous Materials 167: 427-433.
601 Weng L, Temminghoff EJM, van RiemsdijkWH (2001) Contribution of individual sorbents to
602 the control of heavy metal activity in sandy soil. Environmental Science and Technology
603 35: 4436–4443.
604 Xiong J, Koopal LK, Tan W, Fang L, Wang M, Zhao W, Liu F, Zhang J, Weng L (2013)
605 Lead binding to soil fulvic and humic acids: NICA-Donnan modeling and XAFS
606 spectroscopy. Environmental Science and Technology 47: 11634-11642.
607 Xu Y, Bonnfueng T, Axe L, Maeng S, Tyson T (2006) Surface complexation of Pb(II) on
608 amorphous iron oxide and manganese oxide; Spectroscopic and time studies. Journal of
609 Colloid and Interface Science 299: 28-40.
610 Young SD, Zhang H, Tye AM, Maxted A, Thums C, Thornton I (2006) Characterizing the
611 availability of metals in contaminated soils. I. The solid phase: sequential extraction and
612 isotopic dilution. Soil Use and Management 21: 450-458.
613

Figure captions

Figure 1: Pb distribution between the eight fractions defined by the sequential extraction scheme.

Figure 2: Backscattered electron image of a thin section of the S2T soil sample and corresponding elemental maps obtained by EDS. The EDS concentration unit is arbitrary.

Figure 3: SEM images (backscattered electrons; left), EDS (top) and Raman (bottom) spectra recorded on a fir needle (a) and a soil aggregate (b) from S2T and on a leaf fragment from S1T (c). The Raman spectra of the synthetic manganese oxide with and without 5% adsorbed Pb are also displayed. The white squares correspond to the areas where the EDS and RMS spectra were acquired.

Tables

Table 1: Sequential extraction procedure adapted from Laveuf et al. (2009).

Soil fraction	Extractant	Volume (mL)	Conditions
F1: Exchangeable	0.1M $NaNO_3$	10	20°C, 2 hours, end-over-end shaking
F2: Acid-soluble	1M CH_3COONa, pH 5.5 (CH_3COOH 99-100%)	20	20°C, 6 hours, end-over-end shaking
F3: Bound to Mn oxides	0.1M $NH_2OH.HCl$ / 0.1M HCl, pH 2	20	2 times: 20°C, 30 minutes, end-over-end shaking
F4: Easily oxidisable fraction	0.1M $Na_4P_2O_7$, pH 10	10	3 times: 20°C, 90 minutes, end-over-end shaking
F5: Bound to amorphous Fe oxides	0.25M $NH_2OH.HCl$ / 0.25M HCl, pH 1.5.	20	2 times: 60°C, 2 hours, end-over-end shaking
F6: Bound to crystalline Fe oxides	1M $NH_2OH.HCl$ / CH_3COOH 25%, pH 1.	30	2 times: 90°C, 3 hours and 1 hour and half, end-over-end shaking
F7: Oxidisable fraction (sulphurs)	750mg KClO3 in 5 mL 12M HCl and 10 mL 12M HCl	15	20°C, 30 minutes, end-over-end shaking
	4M HNO_3	10	90°C, 20 minutes, end-over-end shaking
F8: Residual	HF-$HClO_4$-HNO_3.	-	-

Table 2: Soil samples characteristics. The SOM is assumed to be 2 times the TOC.

	pH	Pb	Mn	Fe	Clay	Silt	Sand	SOM	CEC
	water	$mg.kg^{-1}$			%			%	$cmol.kg^{-1}$
S1T	4.3	3555	267	18333	21.9	63.3	14.8	17.8	22.5
S1B	4.6	1034	260	19800	20.6	65.5	13.9	10.4	14.7
S2T	4.4	9034	1163	19725	26.1	57.6	16.3	20.6	26.6
S2B	4.5	881	647	19000	22.1	62.3	15.6	9.4	15.4
S3T	4.4	6167	678	26033	49.9	42.0	8.1	49.8	61.9
S3B	4.6	7495	267	27733	45.1	43.8	11.1	47.9	60.4

636 Table 3: Concentrations of reactive sorption surfaces in the soil samples.

Sample	Mineral phases XRD	Clay charge mol.kg^{-1}	Calculated HA g.kg^{-1}	Clay g.kg^{-1}	Amor-Fe g.kg^{-1}	Cry-Fe g.kg^{-1}	Mn oxides g.kg^{-1}
S1T	Quartz 29%; Muscovite 28%; Kaolinite 18%; Chlorite 8%; Illite 17%.	0.15	33.6	219	1.81	5.32	0.02
S1B		0.15	20.3	206	2.25	5.22	0.04
S2T	Quartz 24%; Muscovite 32%; Kaolinite 20%; Chlorite 5%; Illite 18%.	0.16	39.3	261	2.56	5.84	1.29
S2B		0.16	20.8	221	2.43	4.93	0.38
S3T	Quartz 14%; Muscovite 34%; Kaolinite 18%; Chlorite 3%; Illite 30%.	0.19	92.2	499	2.42	5.86	0.63
S3B		0.19	91.2	451	3.38	5.80	0.11

637
638
639
640 Table 4: Modelling of Pb partitioning between the reactive soil solid phases for the 6 soil
641 samples using the generic parameters of Milne et al. (2003) and Xiong et al. (2013). The
642 results are expressed in mg.kg^{-1} and % of total modelled Pb.

	Milne et al. (2003)				
	Pb-Tot mg.kg^{-1}	Pb-HA	Pb-HMO	Pb-HFO	Pb-Clay
S1T	682	638 (93.5%)	5.9 (0.9%)	2.3 (0.3%)	35.9 (5.3%)
S1B	331	299 (90.3%)	12.5 (3.8%)	2.1 (0.6%)	17.5 (5.3%)
S2T	1982	1488 (75.1%)	427 (21.5%)	8.8 (0.4%)	57.7 (2.9%)
S2B	442	316 (71.6%)	110 (24.8%)	2.5 (0.6%)	13.2 (3.0%)
S3T	1488	1287 (86.5%)	183 (12.3%)	2.5 (0.2%)	16.3 (1.1%)
S3B	2035	1968 (96.7%)	32.9 (1.6%)	6.8 (0.3%)	27.2 (1.3%)

	Xiong et al. (2013)				
	Pb-Tot mg.kg^{-1}	Pb-HA	Pb-HMO	Pb-HFO	Pb-Clay
S1T	1790	1746 (97.5%)	5.9 (0.3%)	2.3 (0.1%)	35.9 (2.0%)
S1B	808	776 (96.0%)	12.5 (1.5%)	2.1 (0.3%)	17.5 (2.2%)
S2T	4767	4274 (89.7%)	427 (8.9%)	8.8 (0.2%)	57.7 (1.2%)
S2B	936	810 (86.6%)	110 (11.7%)	2.5 (0.3%)	13.2 (1.4%)
S3T	3379	3178 (94.0%)	183 (5.4%)	2.5 (0.1%)	16.3 (0.5%)
S3B	5468	5401 (98.8%)	32.9 (0.6%)	6.8 (0.1%)	27.2 (0.5%)

643

Figure 1

Click here to download high resolution image

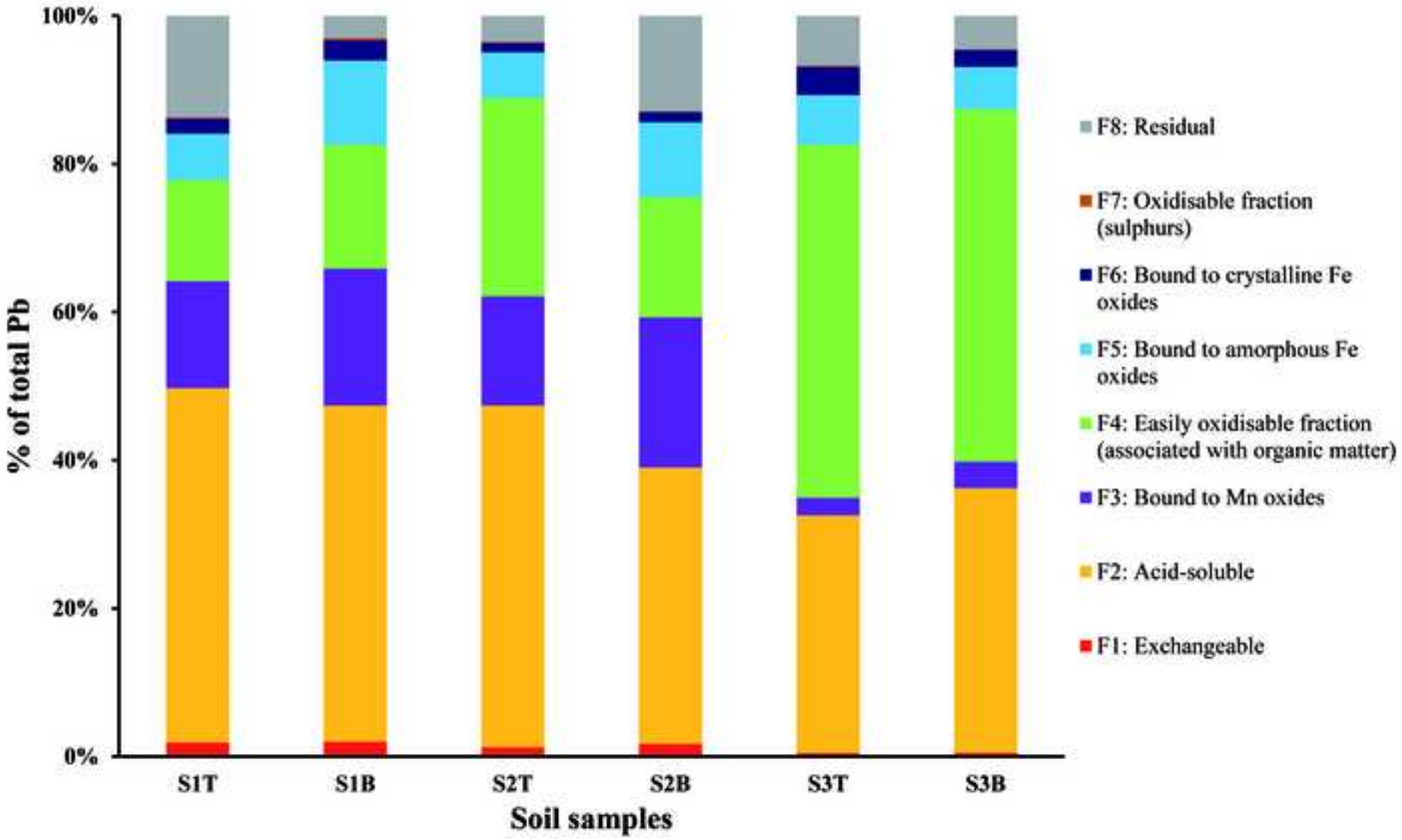

Figure 2

Click here to download high resolution image

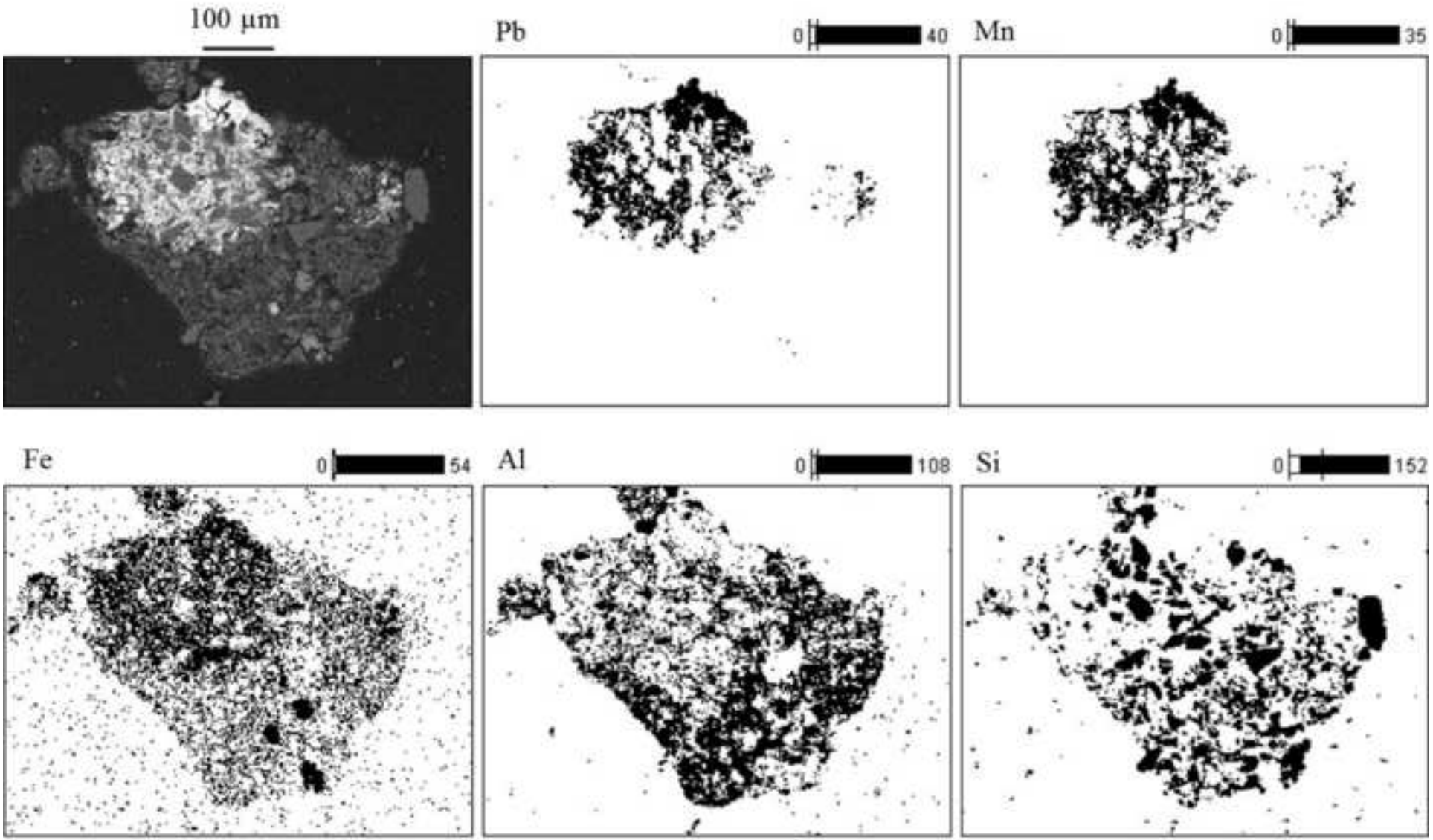

Figure 3

Click here to download high resolution image

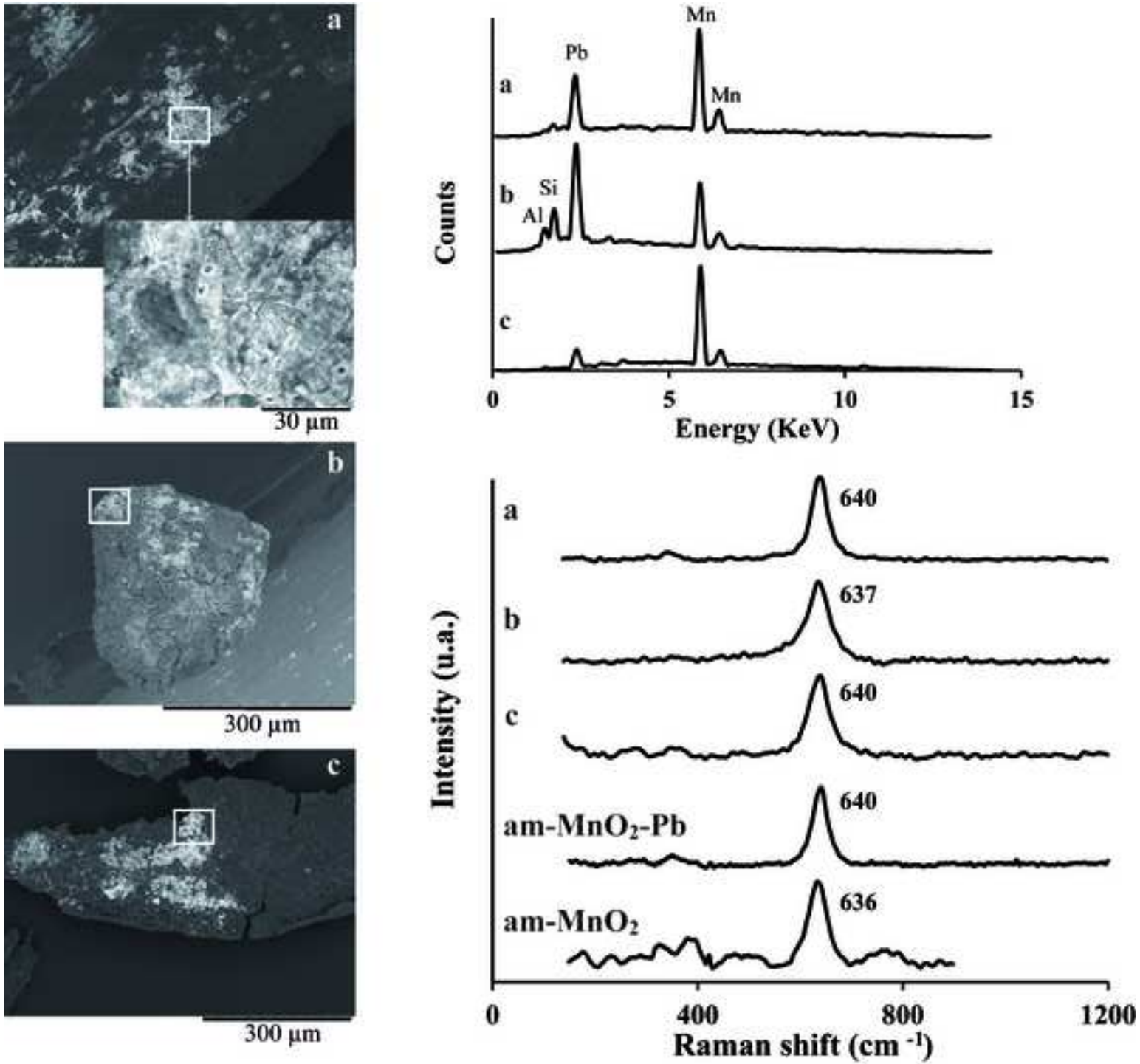

Supplementary material for on-line publication only

Click here to download Supplementary material for on-line publication only: Supplementary materials.docx